Electronic Effects in the Length Distribution of Atom Chains

J. N. Crain, M. D. Stiles, J. A. Stroscio, and D. T. Pierce

Electron Physics Group, National Institute of Standards and Technology, Gaithersburg, Maryland 20899-8412, USA

(Received 7 October 2005; published 17 April 2006)

Gold deposited on Si(553) leads to self-assembly of atomic chains, which are broken into finite segments by defects. Scanning tunneling microscopy is used to investigate the distribution of chain lengths and the correlation between defects separating the chains. The length distribution reveals oscillations that indicate changes in the cohesive energy as a function of chain length. We present a possible interpretation in terms of the electronic scattering vectors at the Fermi surface of the surface states. The pairwise correlation function between defects shows long-range correlations that extend beyond nearest-neighbor defects, indicating coupling between chains.

DOI: 10.1103/PhysRevLett.96.156801 PACS numbers: 73.20.At, 68.37.Ef, 73.21.Hb

In nanostructures, when electrons are confined to dimensions that approach their de Broglie wavelength, the size and geometry of the confinement transforms the electronic structure. In turn the confined electronic states directly impact the energetics of the nanostructures. Such quantum size effects have had profound technological and scientific implications, for example, leading to the interlayer exchange coupling between magnetic multilayers [1,2]. In many cases, the effects of the confined states on the energetics are directly observed through the formation of structures with ''magic'' sizes, such as clusters [3] and thin films at surfaces [4–6].

For nanostructures formed at surfaces, quantum confinement should also play a role in the energetics. However, complications arise since the confinement of states in the lateral dimension is only partial and both strain and substrate electronic states inevitably contribute to the energetics as well. While spectroscopic studies have directly demonstrated the lateral confinement of electronic states within nanostructures such as quantum corrals [7] and atomic chains [8–10], to date most of the experimental work has been limited to the spectroscopy of individual structures and not their energetics. Electronic effects have been observed in the interaction between Cu adatoms on Cu(111) [11] and the stability of small Ag islands [12]. Similarly, recent studies of the Si(111)-(5 × 2) Au surface reconstructions have suggested a link between the electronic structure at the Fermi level and the arrangement of silicon adatoms at the surface [13–16].

In the present study, we explore the role of the electronic states in the energetics of self-assembled atomic chains of Si(553)-Au by analyzing the distribution of chain segments created by atomic defects. We measure both the length distribution of atomic chain segments as well as the pairwise correlation function between atomic defects. The length distribution gives a direct measure of interactions between adjacent defects while the correlation function includes pairs separated by intermediate defects and thus includes interactions that extend beyond isolated segments. We observe oscillations in the length distribution that indicate changes in the cohesive energy with chain length. Further, we find two separate components of the interaction and suggest a possible explanation in terms of the electronic spanning vectors at the Fermi surface. Electrons propagating along a chain are backscattered at defects leading to the formation of quantized states in finite segments [8]. Since the back scattering is not complete, elec-

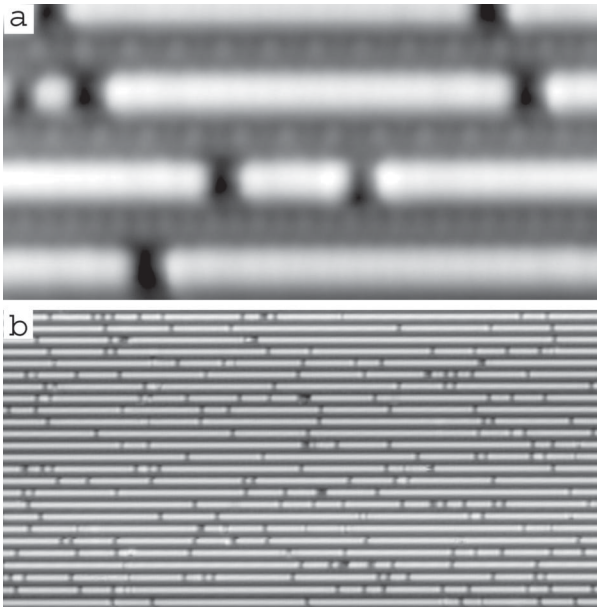

FIG. 1. Scanning tunneling microscopy images show defects and chain segments on the Si(553)-Au surface at low defect density. (a) A 5 nm × 10 nm close-up shows the most common size defects, which are two lattice constants wide and appear as depressions in the chains. (b) A 37.5 nm × 75 nm overview is a subsection of a typical image used to calculate the length distribution and pairwise correlation function. Most of the defects are doublets as in (a), but several larger defects are also observed. Single-atom defects are barely visible. The sample bias is −0.7 V in (a) and −1 V in (b).

tronic states that are transmitted to the next chain segment can lead to interactions that extend beyond isolated segments. The pairwise correlation function between defects shows statistically significant deviations from a calculated pairwise correlation that assumes only interactions between nearest-neighbor defects. By examining the Fourier components of this deviation, we identify interactions that extend beyond those between nearest-neighbor defects.

Atomic chains were fabricated by taking advantage of gold-driven reconstruction of the vicinal Si(553) surface as described in detail in previous studies [17,18]. After flashing the sample clean at 1250 °C, the deposition of gold at about 650 °C led to a self-assembled array of parallel atomic chains. A subsequent anneal to about 830 °C followed by a gradual cooldown over several minutes provides low defect densities. The chains are broken by atomic defects that appear as depressions in scanning tunneling microscopy images leaving chain segments of varying lengths, as shown in Fig. 1. The spatial distribution of chain segments and defects was measured using a custom designed and fabricated scanning tunneling microscope (STM) operated at room temperature. To obtain sufficient statistics, large-scale 50 nm $\times$ 150 nm images were acquired at high pixel density [Fig. 1(b)]. The defect density (average chain length) was observed to increase (decrease) gradually over time during measurements. To determine if the same interactions apply at different densities and to address differences due to the defect formation process [19], we choose images at two densities, low density and medium density, and analyze them separately.

The chain length distributions derived from counting over 3400 chains at low defect density and over 17 000 chains at medium defect density are shown in Figs. 2(a) and 2(b). A completely random distribution of defects positioned along a linear chain yields a distribution of chain lengths $P(n) = \rho(1 - \rho)^n$ that depends only on the density of defects, ρ. Fits to the experimental data yield values for the average chain lengths, determined from the densities in the fits, $\bar{d} = 15.0$ and $\bar{d} = 7.0$ silicon lattice constants for low and medium densities, respectively. These are close to the experimentally determined averages $\bar{d} = 14.9$ and $\bar{d} = 7.3$ [Figs. 2(a) and 2(b)]. Significant deviations from the random distribution are apparent for short chain lengths. To better observe the deviations the experimental data at medium density is normalized by the random distributions [Fig. 2(c)] [20].

Strong oscillations in the normalized distribution indicate fluctuations in the cohesive energy with chain length [Fig. 2(c)]. The distribution is highlighted by three key features. A strong peak at a length of one atom probably arises from short-range interactions, such as the local rebonding of the surface. For longer chains, even chain lengths are favored over odd lengths out to lengths of at least 16 atoms. Finally, a long-range beating in the intensity at a period of roughly eight lattice constants implies a second component to the interactions. All of these features also appear in the normalized distribution at low densities (not shown) indicating the same underlying potential governs both. We would like to emphasize that the size of the oscillations are surprisingly large, up to $\pm 25\%$ in Fig. 2(c), and the corresponding oscillations in the potential energy must be correspondingly large.

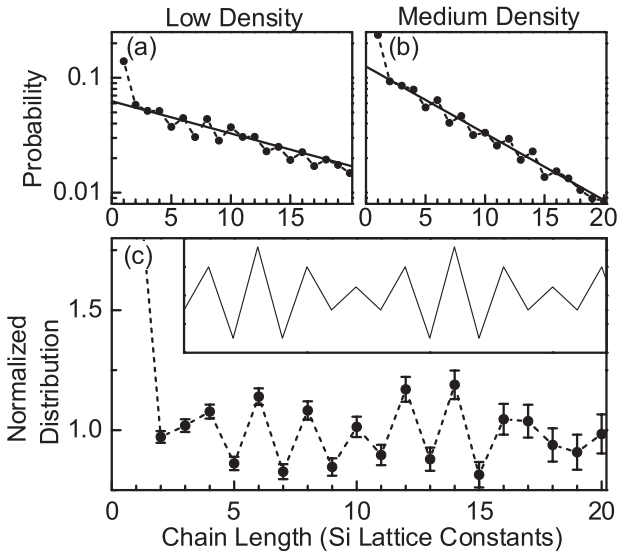

FIG. 2. The probability distribution of lengths for different chain segments was compiled from images similar to that in Fig. 1 for (a) low defect density and (b) medium defect density. A semilog scale is used to better observe small fluctuations and the probability distribution for a random arrangement of defects along a linear chain is shown for comparison (solid curves; see text). (c) The probability distribution at medium defect density is normalized to the random distribution function. For longer lengths, even-odd oscillations as well as a slow beating demonstrate long-range interactions. The inset illustrates the calculated beating between two oscillations at frequencies of 0.375 and 0.5 inverse lattice constants.

The Fermi surface of the Si(553)-Au surface, as measured by photoemission, suggests a plausible link to the observed oscillations in the probability distribution with length [Figs. 3(a) and 3(b)]. Si(553)-Au has three bands, one at just over quarter-filling and a doublet at just over half-filling (See Fig. 1 in Ref. [17]). Since the Fermi surfaces exhibit measurable two-dimensional dispersion, the four allowed scattering vectors between electrons moving in opposite directions at the Fermi level take on a range of possible values [Fig. 3(b)]. The windows of allowed scattering vectors are (0.41–0.46) Å^{-1}, (0.63–0.64) Å^{-1}, (0.67–0.68) Å^{-1}, and (0.76–0.77) Å^{-1}, labeled 1, 2, 3, and 4, respectively, in Fig. 3. The corresponding frequencies, in units of inverse lattice constants, (0.25–0.28), (0.38–0.39), (0.41–0.42), and (0.46–0.47) can be directly compared to the experimental data. Two additional scattering vectors arise between the split bands, (0.71–0.73) Å^{-1} and (0.80–0.81) Å^{-1}, but recent theoretical calculations suggest these are most likely spin forbidden [17,21,22].

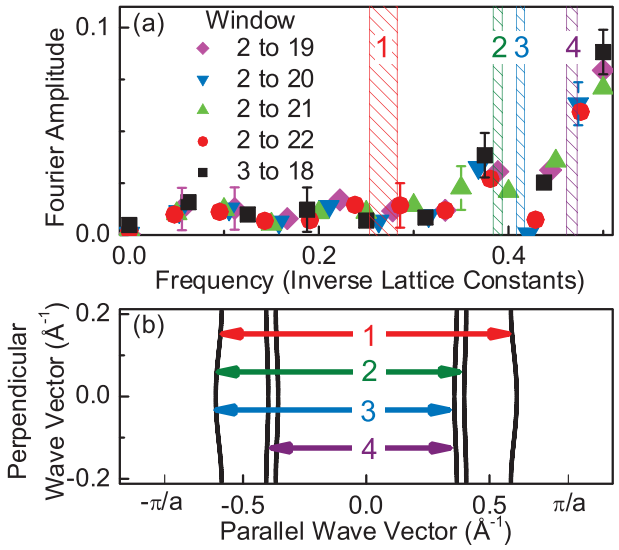

FIG. 3 (color). (a) Fourier transforms using different windows of the normalized length distribution in Fig. 2(c) (colored symbols), for example, the data in the range from 3 to 18 lattice constants (black squares). These are compared with the allowed scattering vectors predicted from the Fermi surface of Si(553)-Au, indicated by the vertical bars. The widths of the bars arise from the two-dimensional dispersion in the Fermi surface that gives a range of allowed scattering vectors. Vectors 2 and 4 provide a plausible electronic origin for the observed fluctuations in the length distribution. (b) Schematic diagram shows the Fermi surface of Si(553)-Au along with the allowed scattering vectors in (a).

The beating between two oscillations at frequencies of 0.375 and 0.5 inverse lattice constants would give rise to a short two-atom period along with an eight-atom beating as observed in the experiment [see the inset of Fig. 2(c)]. These frequencies could plausibly arise from two of the scattering vectors in Fig. 3, vectors 2 and 4. For direct comparison we examine the Fourier transform of the normalized distribution [Fig. 3(a)]. In order to sample a more continuous set of frequencies, we use windows of different sizes with domains starting at two or three lattice constants and ending at 18 to 22 lattice constants (including the peak at one causes too large an asymmetry in the left and right boundaries of the fast-Fourier transform window). The results are insensitive to the choice of window, and by changing the boundaries we demonstrate that the observed features do not arise from boundary asymmetries. The Fourier transform of the normalized length distributions at medium defect density exhibits peaks at frequencies near 0.38 and 0.5 inverse lattice constants, as shown in Fig. 3(a). Thus the Fourier transform provides a plausible link to the electronic structure, with two scattering vectors from the Fermi surface tied to the experimentally observed periods. The absence of the remaining scattering vectors in the data may be attributable to the details of the matrix elements and wave functions, which critically determine the scattering vectors that contribute to the potential.

Electron-electron or electron-phonon interactions may also play a role in transforming the wavelengths of the scattering vectors, as has been shown for electron-electron interactions in the case of chromium [23]. Indeed, since the chains are one-dimensional such interactions are expected to play a key role. For example, the coupling of the electronic states to the lattice can trigger a Peierls-type instability that would enhance the oscillations in the potential or lock them in commensuration with the lattice. Such a Peierls distortion might be manifest in STM images that reveal oscillations in the topography near defect sites, along the valleys between rows, which have a period of two lattice constants (doubled period) [see Fig. 1(a)]. Indeed, a localized lattice doubling was observed in a recent x-ray diffraction study [24]. While a lattice doubling by itself could contribute to the even-odd oscillations in the length distribution [0.5 peak in Fig. 3(a)], it is insufficient to explain the second component of the potential [0.38 peak in Fig. 3(a)] without also invoking a connection to the electronic structure. The data suggest the electronic structure affects the length distribution, but further studies are clearly warranted to understand the role of other interactions.

To distinguish the two-body interactions from many-body interactions that extend beyond isolated segments, we also compute the pairwise correlation function, g_k, between defects. g_k is the probability of finding a defect at site $i + k$ given a defect at site i and, when normalized to the random number of pairs, is given by

$$g_k = N\sum_i (n_i n_{i+k}) \Big/ \Big(\sum_i n_i\Big)^2 \qquad (1)$$

where n_i (either zero or one) is the occupation number of site i and N is the total number of sites [13]. g_k is comple-

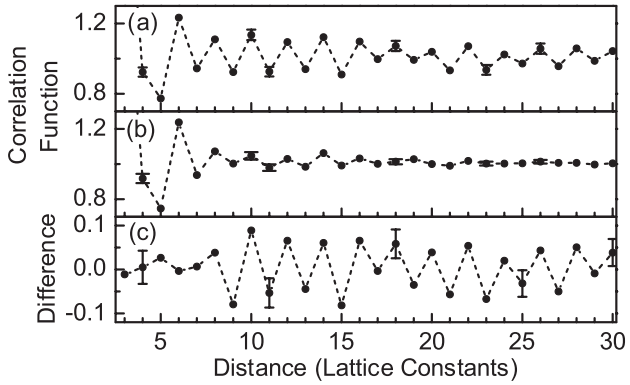

FIG. 4. (a) The pairwise correlation function between doublet defects is obtained from the same data as used in Fig. 2(b) for medium defect density. (b) For comparison, a pairwise correlation function is computed from the length distribution, from Fig. 2(b) but with only doublet defects. (c) The difference between the experimental and calculated correlation functions exhibit extended oscillations with a single dominant period of two lattice constants, indicating interactions that extend beyond adjacent defects [20].

mentary to the length distribution, including higher-order interactions between pairs separated by intermediate defects, which are absent in the length distribution. In computing the pairwise correlation function, we must also consider the size distribution of the observed defects. Approximately 85% of the defects are doublets, and the remainders are mainly singlets, with some triplets, quadruplets, or larger defects [Fig. 1(a)]. To avoid the complications that result from a range of defect sizes, we study only the pairwise correlation function between doublets. We compare the correlation function at medium density [Fig. 4(a)] to the correlation function expected from the measured length distribution, which assumes only interactions between neighboring defects [Fig. 4(b)]. This is computed by starting from the probability distribution of distances between neighboring defects (the length distribution) and summing the probabilities for all of the possible configurations at each given separation. The length distribution is from Fig. 2(b), except in order to sample the same distribution as used in the correlation function we look at only the lengths between adjacent two-atom defects.

The pairwise correlation function exhibits oscillations as a function of length that extend further than predicted from the length distribution alone. While in the experimental pairwise correlation function [Fig. 4(a)] the oscillations extend further than 40 lattice constants, they drop off rapidly in the length distribution derived correlation function [Fig. 4(b)]. The deviation is best seen by taking the difference between the experimental and calculated distributions [Fig. 4(c)], which exhibits a dominant oscillation at a period of two lattice-constants. This is confirmed by the Fourier transform of the difference (not shown), which reveals a single peak at a frequency near 0.5 inverse lattice constants with the peak near 0.38 inverse lattice constants notably absent. Since both frequencies were present in the length distribution, this implies two separate components of the interactions with one component at a period of two lattice constants that extends beyond isolated chain segments along the rows [25]. The defect formation process might also lead to extended oscillations with only nearest-neighbor interactions, since defects are added to a preexisting ordered array. However, the oscillations in STM topography near defects [Fig. 1(a)] have a two-atom period that matches the oscillations in the correlation function and extend beyond adjacent defects. This period doubling provides further evidence for a single component of the interactions that extends beyond adjacent defects, either arising from long-range Friedel type oscillations in the potential or an accompanying lattice instability pinned near defect sites.

This work was supported in part by the Office of Naval Research.

[1] M. D. Stiles, Phys. Rev. B **48**, 7238 (1993).
[2] J. Unguris, R. J. Celotta, and D. T. Pierce, Phys. Rev. Lett. **79**, 2734 (1997).
[3] W. A. Deheer, Rev. Mod. Phys. **65**, 611 (1993).
[4] D. A. Luh, T. Miller, J. J. Paggel, M. Y. Chou, and T. C. Chiang, Science **292**, 1131 (2001).
[5] Z. Y. Zhang, Q. Niu, and C. K. Shih, Phys. Rev. Lett. **80**, 5381 (1998).
[6] R. Otero, A. L. V. de Parga, and R. Miranda, Phys. Rev. B **66**, 115401 (2002).
[7] M. F. Crommie, C. P. Lutz, and D. M. Eigler, Science **262**, 218 (1993).
[8] J. N. Crain and D. T. Pierce, Science **307**, 703 (2005).
[9] S. Folsch, P. Hyldgaard, R. Koch, and K. H. Ploog, Phys. Rev. Lett. **92**, 056803 (2004).
[10] N. Nilius, T. M. Wallis, and W. Ho, Science **297**, 1853 (2002).
[11] J. Repp, F. Moresco, G. Meyer, K. H. Rieder, P. Hyldgaard, and M. Persson, Phys. Rev. Lett. **85**, 2981 (2000).
[12] K. Morgenstern, E. Laegsgaard, and F. Besenbacher, Phys. Rev. Lett. **94**, 166104 (2005).
[13] A. Kirakosian, R. Bennewitz, F. J. Himpsel, and L. W. Bruch, Phys. Rev. B **67**, 205412 (2003).
[14] J. L. McChesney, J. N. Crain, V. Perez-Dieste, F. Zheng, M. C. Gallagher, M. Bissen, C. Gundelach, and F. J. Himpsel, Phys. Rev. B **70**, 195430 (2004).
[15] H. S. Yoon, S. J. Park, J. E. Lee, C. N. Whang, and I. W. Lyo, Phys. Rev. Lett. **92**, 096801 (2004).
[16] S. C. Erwin, Phys. Rev. Lett. **91**, 206101 (2003).
[17] J. N. Crain, A. Kirakosian, K. N. Altmann, C. Bromberger, S. C. Erwin, J. L. McChesney, J. L. Lin, and F. J. Himpsel, Phys. Rev. Lett. **90**, 176805 (2003).
[18] J. N. Crain, J. L. McChesney, F. Zheng, M. C. Gallagher, P. C. Snijders, M. Bissen, C. Gundelach, S. C. Erwin, and F. J. Himpsel, Phys. Rev. B **69**, 125401 (2004).
[19] Defects added to an existing defect array at room temperature might exhibit different energetics than for those created during the self-assembly process.
[20] The 1 standard deviation error bars shown were calculated assuming $\sqrt{N}$ statistics. The validity of this approximation was supported by the standard deviations in the distribution taken from different images at the same defect density.
[21] S. LaShell, B. A. McDougall, and E. Jensen, Phys. Rev. Lett. **77**, 3419 (1996).
[22] D. Sanchez-Portal, S. Riikonen, and R. M. Martin, Phys. Rev. Lett. **93**, 146803 (2004).
[23] R. S. Fishman, Phys. Rev. Lett. **81**, 4979 (1998).
[24] S. K. Ghose, I. K. Robinson, P. A. Bennett, and F. J. Himpsel, Surf. Sci. **581**, 199 (2005).
[25] To test the role of two-dimensional interactions we also measure the pairwise correlation function between two-atom defects in adjacent rows (not shown). Peaks in the correlation function between rows were 5 times smaller than along the chain and thus interactions along the chain appear dominant, as is expected from the highly anisotropic band structure.